



Quantifying irreversible movement in steep fractured bedrock permafrost at Matterhorn (CH)

Samuel Weber¹, Jan Beutel², Jérôme Faillettaz¹, Andreas Hasler³, Michael Krautblatter⁴, and Andreas Vieli¹

¹Department of Geography, University of Zurich, Switzerland

²Computer Sciences, ETH Zurich, Switzerland

³Department of Geosciences, University of Fribourg, Switzerland

⁴Landslide Research, Technical University of Munich, Germany

Correspondence to: Samuel Weber (samuel.weber@geo.uzh.ch)

Abstract. Identifying precursors of gravity-driven slope instabilities in inhomogeneous fractured rock masses is a challenging task. Recent laboratory studies have brought upon an enhanced understanding of rock fatigue and fracturing in cold environments but were not successfully confirmed by field studies. In this study we monitor environmental conditions, rock temperatures and fracture dynamics at 3500m a.s.l. on the steep, strongly fractured Hörnligrat of Matterhorn (Swiss Alps). Here we analyze seven years of continuous data of the long term evolution of fracture dynamics in permafrost offering unprecedented level of detail and observation duration. The fracture dynamics consists of reversible and irreversible movement components resulting from a combination of temporal varying driving and resisting forces. As irreversible motion is suspected to occur prior to global gravity-driven slope failure, we developed a statistical model, assuming the reversible deformation is caused by thermo-mechanical induced strain, and tested it successfully with field measurements from steep permafrost bedrock. We apply this linear regression model to our data set of fracture dynamics and rock temperature in order to separate the residual irreversible movement component. From this, we produce a new metric that quantifies relative irreversibility of fracture dynamics and enables a better interpretation of the data. This index of irreversibility is based on in situ measurements and enables a local assessment of rock wall stability. Here we show how environmental forcing causes reversible and irreversible rock mass deformations that might be relevant in preconditioning rock slope instability. In general, all locations instrumented show a trend of fracture opening, but at variable rate between locations. At each individual location, the temporal pattern of deformation is very similar every year. All but one sensors show a reversible deformation component caused by thermo-mechanical induced strain. For many sensors, we observe an irreversible enhanced fracture deformation in summer, starting when rock temperatures reach above zero. This likely indicates thawing related process, such as melt water percolation into fractures, as a forcing mechanisms for irreversible deformation. Most likely, such water or thawing leads to a decrease of the cohesion and friction along fracture in the shear zone. For a few fractures instrumented, we find an irreversible deformation with the onset of freezing period, which suggest that cryogenic processes act as a driving factor through increasing ice pressure. It further highlights that irreversible fracture deformation can even at locations in close proximity not be explained by one single process.



Keywords

Fracture dynamics, steep bedrock permafrost, high mountain permafrost, fracture monitoring

1 Introduction

On steep high-alpine mountain slopes, the behavior of frozen rock mass is an important control of slope stability when permafrost warms or thaws and seasonal frost occurs. During the hot summer of 2003, air temperatures across a large portion of Europe were 3°C warmer than the 1961–1990 average (Schär et al., 2004), causing deep thaw and coinciding with exceptional rockfall activity in the European Alps (Gruber et al., 2004). In the last century, the upper tens of meters of Alpine permafrost in Europe have been observed to warm by $0.5 - 0.8^{\circ}\text{C}$. Assuming that this warming continues or even accelerates, gravity-driven slope instabilities are expected to become increasingly important for scientists, engineers and inhabitants in the vicinity of high mountain permafrost regions (Gruber and Haeberli, 2007; Keuschnig et al., 2015). A coexistent growth of vulnerable socio-economic activities in alpine areas potentially leads to rising risk (Jomelli et al., 2007). In the USA and Europe, gravity-driven slope instabilities cause damage in the range of billions of euros each year (Sidle and Ochiai, 2006). An improved assessment and monitoring strategies for frozen rock walls is therefore needed and requires better understanding of processes and factors controlling slope stability of potentially hazardous slopes.

Terzaghi (1962) postulated that the stability of steep unweathered rock slopes is determined by the mechanical defects of the rock such as joints and faults and not by the strength of the rock itself. In cold regions, rock is exposed to frost cycles of variable length (Haeberli, 1996), leading to mechanical rock damage caused by different processes, such as thermal gradients (Hall et al., 2002) or cryostatic pressure (Walder and Hallet, 1985). Ice formation is known to be an important driver of rock fracturing and can be produced by ice expansion or ice segregation. These two processes have been widely discussed, but it remains difficult to incorporate this knowledge with field observations (Matsuoka and Murton, 2008). Ice formation induces pressure variations in rock pores and cracks at a level that is sufficient to crack intact high porosity rocks (Murton et al., 2006). Ice-filled joints hereby developed may inherit relatively tough ice bodies at low temperatures with the shear resistance decreasing with rising temperature and reaching a minimum just below the thawing point (Davies et al., 2001). When intact water-saturated rock thaws, fracture toughness and compressive and tensile strength decrease by up to 50% (Krautblatter et al., 2013). Besides the relatively slow process of heat conduction, the warming of frozen fractured bedrock is influenced by advective heat transport by percolating water, which efficiently transfers heat from the surface to the level where fractures become impermeable (Hasler et al., 2011). Such advective heat transport produces rapid variations in mechanical properties, which can potentially deform frozen discontinuities and consequently prepare rock-slope failures.

Assessing and anticipating rock wall stability is a challenging task, mainly because of the incomplete understanding of precursory signals and the inherent mechanical complexity of fractured inhomogeneous rock and ice masses (Arosio et al., 2009). Measuring surface displacements has been applied widespread to survey fracture deformation in permafrost revealing a clear temperature dependent reversible component related to thermal expansion (Wegmann and Gudmundsson, 1999; Matsuoka and Murton, 2008; Nordvik et al., 2010; Hasler et al., 2012; Blikra and Christiansen, 2014). Slope failure is the final stage of



irreversible motion, resulting from a disbalance between driving and resisting forces. Reversible and irreversible motion are often superimposed and therefore it is difficult to interpret deformation data and relate to external forcing factors.

This study presents a statistical model for computing the reversible thermo-mechanical induced fracture dynamics in steep bedrock permafrost derived from measured fracture deformation. This approach allows to separate the irreversible movement components and to investigate the dynamics of fractures in ice-rich fractured bedrock permafrost with focus on enhanced fracture opening and shearing observed during summer. Irreversible movement refers to slow slope deformation, which is seen as a part of slope instability, potentially preparing slope failure. This statistical model has been developed and tested using 7 years of continuous high resolution temperature and fracture deformation measurements from the Matterhorn Hörnligrat, a high mountain permafrost monitoring site. This study addresses three main questions:

1. How can we separate reversible from irreversible fracture movements by statistical means?
2. Is there a common inter-annual pattern of irreversible fracture movement at all fractures instrumented?
3. What kind of environmental conditions lead to enhanced irreversible motion?

In the first part of this paper we illustrate a conceptual model that describes fracture dynamics in steep fractured bedrock permafrost (Section 2) and describe a novel field measurement setup (Section 3). We pinpoint a quantitative way to distinguish between reversible and irreversible movement by temperature dependent statistical analysis and model (Section 4). This approach is used to analyze the data set comprising seven years (Section 5). We further elaborate on inter- and intra-annual fracture dynamics and finally build and discuss a new index of irreversibility, a novel metric providing useful indications on rock wall stability.

2 Conceptual model

Surface displacements in steep fractured bedrock permafrost could reflect environmental processes controlled by temporally varying environmental forcing. To better isolate the individual processes, it is necessary to separate them in space and time as well as to relate them to the forcing mechanisms. Based on the rock-ice-mechanical model of Krautblatter et al. (2013), a new conceptual model of permafrost affected slope instabilities in steep fractured bedrock is proposed, sketched out in Fig. 1. This model tries to link spatial and temporal patterns of movements to related processes. Herein topographically controlled gravitational forces (D1), thermo-elastic induced strains (D2), ice pressure (D3) and hydrostatic pressure (D4) act as driving forces. Resisting forces are composed of cohesion and friction along fractures (R1), shear resistance of cohesive rock bridges (R2), creep and fracture of ice (R3) and the fracture infill (R4). The driving and resisting forces strongly depend on fluctuating environmental as well as static geological/geotechnical characteristics. As long as the driving forces are compensated by the resisting forces, there is no relative motion. But if the forces become unbalanced, either by increasing the driving force or by decreasing the resisting force, deformation occurs.

In general, the motion observed, consisting of reversible and irreversible movement components, results from a combination of several forces. When looking at each of these driving forces separately, it is possible to obtain *rock temperature – fracture*



5 *deformation relations* (see plots in Fig. 1a) for different environmental conditions. The gravitational loading is constant with time and temperature independent and the thermo-elastic induced strain is expected to cause cycles in fracture deformation that are linearly related to temperature. Ice pressure induced forcing only occurs at negative temperature while hydrostatic pressure acts at positive temperature. These relationships between temperature and process in combination with environmental forcing allow to interpret the observed movement patterns.

Short-lived *thermo-elastic induced strains* (D2) accommodate volume changes as movements, typical for fractured bedrock in non-permafrost (Watson et al., 2004) as well as in permafrost areas (Hasler et al., 2012) and is therefore an irreversible process. This volumetric expansion results in a change of length ΔL of rock in all directions that can theoretically be described, assuming homogeneous thermal conditions, by

$$10 \quad \Delta L = L_0 \cdot \alpha \cdot \Delta T \quad (1)$$

where L_0 is the initial length, α the material dependent linear expansion coefficient and ΔT the temperature change of the material. This formula is difficult to apply in real world due to anisotropy and heterogeneity of the rock mass, complex 3D temperature regimes and the unknown behavior of fractured bulk rock masses as well as the fact that rocks with ice-filled porosity might have a non-linear expansion coefficient (Jia et al., 2015).

15 Several studies in permafrost bedrock with different measurement setups (e.g. Wegmann and Gudmundsson, 1999; Matsuoka, 2001; Matsuoka and Murton, 2008; Nordvik et al., 2010) report a correlation between fracture deformation and (rock-) temperature at different time scales from diurnal to annual. Nordvik et al. (2010) applied a multiple regression analysis with aggregated sinusoidal air temperature to model the seasonal fracture dynamics. They propose this approach for predictions of fracture dynamics in context of early warning system.

20 In the long term, deformations along fractures act to change the persistent gravitationally-induced stress distribution in the rock mass controlled by the bulk material stiffness and rock mass strength properties. Creep and fracture of ice (R3) can absorb pressures along fractures and lead to stress reduction (Matsuoka, 1990) while fracture infill (R4) by debris or fine grained material can significantly alter shear resistances of fractures in a frozen or unfrozen state. Persistent thermo-elastic oscillations of an initially stable rock mass (stable phase in Fig. 1b), in combination with an increase of shear stress due to accumulation/concentration of stress at remaining rock bridges or a decrease of shear resistance, leads to irreversible surface displacement (unstable phase in Fig. 1b). Therefore, irreversible deformation is assumed to be a first indication for the initiating of slope failure.

25 *Fracture of cohesive rock bridges* (R2) is temperature dependent and get influenced by warming during slow deformations (Krautblatter et al., 2013). Mellor (1973) showed a significant reduction in strength when frozen rock thaws. Periodic loading of discontinuities due to thermo-mechanical effect acts as a mesoscale fatigue process, which can result in deformation and progressive rock slope failure (Gischig et al., 2011). After a certain fatigue life, tensile and compressive strength reduce to residual values (Jia et al., 2015). Repeated stress on fractures caused by cryogenic processes in permafrost can also lead to fatigue. Deformation in partly frozen rock masses may also be caused by increasing *ice pressure* (D3) evolving in ice-filled fractures or pores by cryogenic processes. Hereby, volumetric expansion or ice-segregation are the most common explanations.

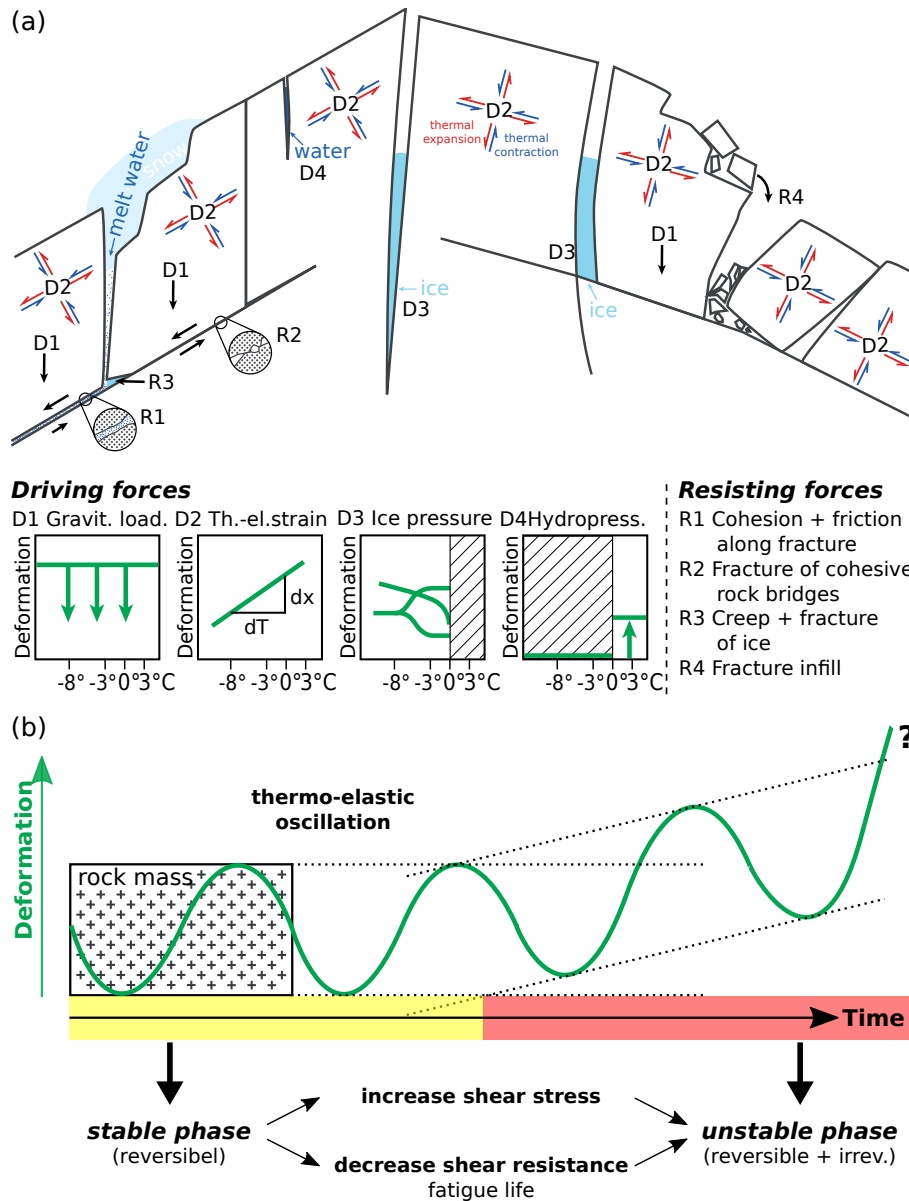


Figure 1. Conceptual model of permafrost affected slope instabilities in steep fractured bedrock. (a) Cross-section through a fractured rock ridge in an alpine environment (top) and the acting environmental forcing (bottom) to describe the relative fracture deformation, as a result of driving and resisting forces. Each driving force causes a specific motion pattern, which is illustrated with the schematic plots showing the relation between rock temperature and fracture deformation. (b) In long term, initially reversible deformation of rock mass can develop an additional irreversible component either by an increase of shear stress or by a decrease of shear resistance.



Volumetric expansion in laboratory experiments is only effective if freezing leads to sealing of fractures of rock fractures or porous samples before ice can extrude (Davidson and Nye, 1985). However volumetric expansion also works in pores which are on average saturated much less than 91 per cent, but due to the unequal moisture distribution, always some pores will have a higher saturation and thus have insufficient space for the volumetric expansion of freezing water (Jia et al., 2015).

5 Ice segregation, which is most effective between -3° and -6° C with sustained water supply (Hallet et al., 1991), describes the freezing of the migrated water at the freezing site, which results in lenses or layers of segregated ice due to ice growth (Matsuoka and Murton, 2008).

Irreversible deformation caused by hydro related processes can only be observed in summer, because the availability of liquid water is very limited during winter. On the one hand, water can act as the driving force through *hydrostatic pressure*

10 (D4), which describes the fluid pressure in rocks, mostly determined by the height of the water column. It depend amongst other factors on hydraulic permeability of the rock mass, which is much lower in rock mass with frozen fissures than unfrozen fissures and often causes high hydrostatic stress levels due to perched water (Pogrebiskiy and Chernyshev, 1977). But there are no detailed empirical quantitative studies on how hydrostatic pressure affects rock walls in permafrost regions (Krautblatter et al., 2013). However, hydrostatic pressure is supposed to not be dominating in the surface layer of strongly fractured steep

15 bedrock, where the ability to drain is quite high. On the other hand, water can change the resisting force *cohesion and friction along a fracture* (R1), which is elementary in steep fractured bedrock. Changing conditions in the shear zone, e.g. dry-wet, can lead to irreversible motion, for example caused by water percolating due to melting snow or rain. This is expected to have a strong influence at fractures filled with fine-grained material.

Based on this conceptual model, we postulate that (i) rock movements can be separated into reversible and irreversible move-

20 ments, (ii) reversible thermo-elastic strains occur during the whole year, (iii) irreversible cryogenic deformations dominantly occur during freezing periods and (iv) irreversible hydro deformations during summer months and periods of snow melt. Using the continuous 7 year deformation and temperature data set, these statements are validated.

3 Site description, instrumentation and field data

The relative fracture displacement and thermal conditions were measured at Matterhorn Hörnligrat (Swiss Alps) at an altitude

25 of 3500m a.s.l. (see Fig. 2). The field site is predestined for such measurements due to: (1) occurrence of ice-filled fractures indicated by an ice-containing scarp after a block fall event (approx. 1500m^3) in summer 2003, (2) strong fracturing, (3) obvious indicators of rock deformation and (4) large gradient of surface thermal conditions allowing installation of thermistors and crackmeters at locations with contrasting conditions (cf. Hasler et al., 2012).

This field site is heterogeneous with partially debris covered ledges in steep fractured bedrock. The precipitation almost ex-

30 clusively falls as snow with occasional infrequent rainfall events in summer. Cold winter temperature in combination with exposure to strong wind result in a preferential snow deposition, in fractures, on ledges and at other concave micro-topographical features. These factors lead to a complex temperature regime due to variable surface characteristics with temporal variations



and therefore need a correspondingly large amount of precisely measured data (Krautblatter et al., 2012). The accumulated firn disappears completely on the south side during summer while snow patches persist on the north side all year.

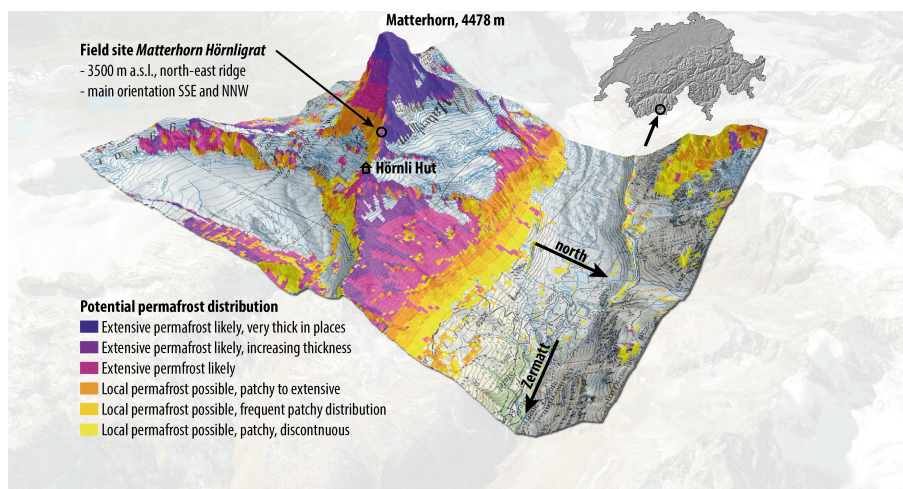


Figure 2. 3D overview of field site Hörnligrat, north-east ridge of Matterhorn, located in Valais, Switzerland (based on map.geo.admin.ch, Google Earth and SRTM). Colors indicate the potential permafrost distribution (FOEN, 2005). At this field site, extensive permafrost with a thin active layer is expected on the north side of the ridge. On the south side of the ridge, local permafrost is possible with a considerable active layer.

In this study three types of data were recorded at different locations: relative fracture deformation perpendicular to and along fractures in a 2 min interval (accuracy of 0.01 mm), temperature at different depths in rock in a 2 min interval (from surface
5 down to 85 cm; accuracy of $\pm 0.2^\circ\text{C}$) and high resolution images (12.0 MP, which gives an approximate pixel resolution of 1.5 cm) 7 times per day. Fracture deformation perpendicular to the fracture are measured at locations *mh01–mh04* while fracture deformation perpendicular and parallel to the fracture are measured at locations *mh06*, *mh08* and *mh20–mh22*. Rock temperature measurements at 85 cm depth are available at locations *mh02–mh04* and *mh10–mh12*. Figure 3 gives a spatial overview of all measurement locations. Basic meta information of the measurement locations are given in Table 1 for the three
10 locations with only temperature and in Table 2 for all crackmeter locations. If there is no co-located temperature measurement, a nearby measurement with similar topography is used. All sensors are embedded in a low power wireless sensor network that provides all year-round data at near real-time (Beutel et al., 2009). The raw temperature and fracture deformation measurements were aggregated as 10 min averages to reduce noise. A detailed description and explanation of the measurement setup, data processing as well as filtering is given by Hasler et al. (2012, Section 3).

15 Instrumentation started in autumn 2007 and continuous time series are available since summer 2008 for locations *mh02*, *mh03* and *mh06*. The measurement network was extended in Summer 2010 with additional sensors and by establishing new measurement locations (*mh01*, *mh04*, *mh08* and *mh20–mh22*). This results in up to 7 years of data.

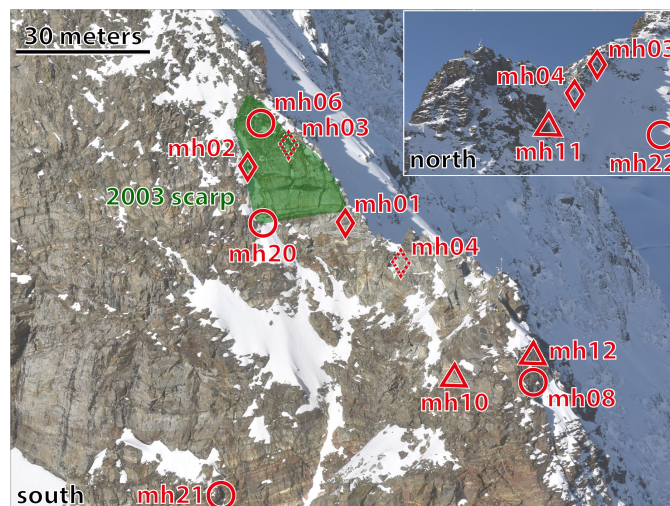


Figure 3. Overview of crackmeter installations. Location *mh01–mh04* (indicated with \diamond) are instrumented with one crackmeter perpendicular to the fracture. Location *mh06*, *mh08* and *mh20–mh22* (indicated with \circ) are instrumented with two crackmeters to calculate motion perpendicular to and along fracture. Rock temperature measurements exist at most location. Location with only temperature measurements are indicated with \triangle . Scarp or the 2003 rockfall is indicated with green.

Table 1. Meta information for temperature locations.

Location	Aspect	Slope	Thermistors at	Label
<i>mh10</i>	140° N	90°	10, 35, 60, 85 cm	T _{south}
<i>mh11</i>	340° N	70°	10, 35, 60, 85 cm	T _{north}
<i>mh12</i>	45° N	90°	10, 35, 60, 85 cm	T _{east}

4 Analysis method

4.1 Temperature gap filling

Gaps in the time series of temperature sensors can occur due to interrupted power supply. To fill long gaps in the temperature time series at 85 cm depth, we apply quantile mapping using best regressor approach (Staub et al., 2015, in review). To select a representing reference time series, we look for measurement locations with similar properties, i.e. altitude, exposition, slope and surface conditions.

4.2 Linear regression model (LRM)

To quantify the temperature dependent reversible component of the fracture dynamics, we modify the approach of Nordvik et al. (2010). Instead of air temperature, we use rock temperature T_{rock} at 85 cm depth. For each measurement location, we then



Table 2. Meta information for crackmeter locations with associated rock temperature. If there is no co-located temperature measurement, a nearby measurement with similar topography is used. Rock temperature refers to measurements at approx. 85 cm depth.

Location	Aspect	Slope	Crackmeter	Rock temperature
<i>mh01</i>	95° N	75°	1 axis	@ location <i>mh10</i>
<i>mh02</i>	8° N	50°	1 axis	<i>mh02</i>
<i>mh03</i>	350° N	65°	1 axis	<i>mh03</i>
<i>mh04</i>	320° N	70°	1 axis	<i>mh04</i>
<i>mh06</i>	90° N	60°	2 axes	@ location <i>mh10</i>
<i>mh08</i>	50° N	90°	2 axes	@ location <i>mh12</i>
<i>mh20</i>	70° N	70°	2 axes	@ location <i>mh02</i>
<i>mh21</i>	70° N	85°	2 axes	@ location <i>mh10</i>
<i>mh22</i>	70° N	85°	2 axes	@ location <i>mh11</i>

apply a linear regression function with rock temperature T_{rock} and model the reversible fracture deformation y_{lrn} :

$$y_{\text{lrn}} = \beta_0 + \beta_1 \cdot T_{\text{rock}} + e_i \quad (2)$$

where β_0 and β_1 are the unknown regression parameters for a fracture, t_i is the time and e_i is the residual.

The temperature values were smoothed with a running window over seven days to reduce the noise, which likely represents temperature at greater depth. The length of the trainings windows get optimized iteratively for each location by searching for the best correlation coefficient, whereby the training window length is constraint to be between 3 months and one year. We also prefer training windows for which the temperature range from -3 to -6°C is passed very rapidly for excluding fracture deformation by ice segregation (Fig. 1, D3). Note that the resulting best training windows periods occur during winter time with temperature below zero. For each fracture instrumented, the optimized correlation coefficient is used for the whole time series in order to model the reversible fracture deformation by thermo-mechanical induced strain.

4.3 Irreversibility index

We build a metric (termed irreversibility index) that aims at detecting periods when overall motion is not dominated by thermo-elastic induced strains. This index uses the raw fracture data (y_{raw}) after removing the modeled reversible fracture dynamics component (y_{lrn}) given by the LRM as input. This difference between y_{raw} and y_{lrn} is applied to running mean values (28 day window length) to reduce noise:

$$y_{\text{diff}} = |\text{runmean}_{28 \text{ days}}(y_{\text{raw}} - y_{\text{lrn}})| \quad (3)$$

where the function $\text{runmean}_{X \text{ days}}$ is evaluated as the centered running mean over all data points in the time window $\pm \frac{X}{2}$ days. Finally, the index is calculated from the difference between the running maximum and running minimum of y_{diff} over 7 days to



reduce fluctuations:

$$\text{index}_{\text{irreversibility}} = \text{runmax}_{7 \text{ days}}(y_{\text{diff}}) - \text{runmin}_{7 \text{ days}}(y_{\text{diff}}) \quad (4)$$

The output value of the irreversibility index is a positive number of unit mm/year. A value at zero means that the motion is fully reversible. The higher the number, the higher is the proportion of irreversibility. The benefit of this approximation is the
 5 temporal sensitivity to the intra-annual fracture dynamics and can therefore be used to detect unstable time periods.

4.4 Thawing degree days (TDD) and fracture dynamics summer offset (OFST)

A thawing degree day model takes into account the amount of energy available for melting over the course of the year (Huybrechts and Oerlemans, 1990). It is here used as a rough approximation the total energy available for melting ice or thawing permafrost. The thawing degree day sum (TDD) is defined as the total sum of daily average rock temperature above 0°C over
 10 one year.

The fracture dynamics summer offset y_{OFST_i} represents the movement between two winters due to creeping and is calculated as:

$$y_{\text{OFST}_i} = \bar{y}_{\text{raw, winter}_{i+1}} - \bar{y}_{\text{raw, winter}_i} \quad (5)$$

with the mean fracture deformation during winter given by

$$15 \quad \bar{y}_{\text{raw, winter}_i} = \sum_{k=t_1}^{t_2} y_{\text{raw}}/n \quad (6)$$

where $t_1 = \text{Nov } 1, \text{ year}_{i-1}$, $t_2 = \text{date}(T_{\text{rock}} < -1^\circ \text{C}) | \text{May } 1, \text{ year}_i$ and n the number of measurements.

4.5 Linear regression model plus (LRM+)

The presented LRM only describes the thermo-elastic induced reversible deformation and does not include an irreversible behavior. The *Linear regression model plus (LRM+)* aims to reproduce the total fracture deformation. It is a combination of
 20 the LRM ($y_{\text{lr}}m$) and periods of linearly approximated irreversible deformation. For a specific time period in winter, which we refer as the reversible phase ($P_{\text{reversible},i}$), we assume that deformation by the thermo-mechanical induced strain dominates. For the residual time period each year, which we refer as the creeping phase ($P_{\text{creep},i}$), we assume that the irreversible movement is active and linear during the whole creeping phase.

The deformation trend function $\hat{y}(\text{data})$ (see Fig. 4) is constant every winter during the reversible period $P_{\text{reversible},i}$, ranging
 25 from $t_{\text{reversible},i,\text{beg}}$ to $t_{\text{reversible},i,\text{end}}$, with the first available data point (see blue point) at the beginning of every year. The beginning of the reversible phase is essentially constraint by the start date of the earlier determined training period (see Section 4.2). There are two option for the end, either by the end of the hydrological year or when the rock temperature cross a defined threshold value of -1°C . The hydrological year approach is suitable for locations where the irreversible deformation is likely caused by cryogenic processes while the temperature threshold approach is applicable for locations melt water related fracture



deformation. The deformation trend function $\hat{y}(\text{data})$ for the creeping phase $P_{\text{creep},i}$ then get piecewise linearly interpolated from the end of a reversible period ($P_{\text{reversible},i}$) to the beginning of the next reversible period ($P_{\text{reversible},i+1}$).

Super-imposing the reversible component of the LRM (y_{lrn}) on the irreversible piecewise linear trend, which is the difference between the deformation trend of the raw data $\hat{y}(\text{raw})$ and the deformation trend of the modeled reversible data $\hat{y}(\text{lrn})$, results in the enhanced LRM+:

$$y_{\text{lrn}+} = y_{\text{lrn}} + \hat{y}_{\text{raw}} - \hat{y}_{\text{lrn}} \quad (7)$$

The resulting piecewise linear function represents the combination of reversible fracture deformation due to thermo-elastic induced strains and enhanced seasonal irreversible linear creep. Note that this model assumes a constant reversibility every year and all irreversible deformation is linear during the creeping phase.

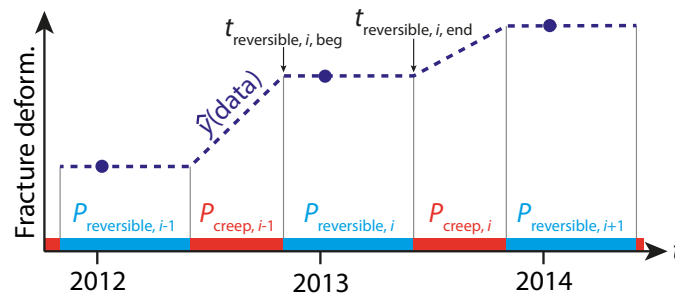


Figure 4. Schematic illustration how the piecewise linear deformation trend function $\hat{y}(\text{data})$ for the LRM+ get determined.

10 5 Results and interpretation

Figure 5 shows the rock temperature at 85 cm depth for different exposition and the fracture dynamics, set to zero at start of measurement, of all locations perpendicular to the fractures and parallel to the fracture. A partly reversible movement can be observed at all locations with different seasonal amplitudes, except for location *mh02*. Most of them also show a long term trend indicating an additional irreversible component. The individual deformation pattern of each location may be influenced by differences in geometric mesoscale arrangement of rock, where different combinations of processes dominate. An irreversible deformation is indicated at most locations in early summer (e.g. *mh02–mh04*, *mh06*, *mh08* and *mh20*) but the exact timing and pattern is difficult to quantify. The fracture dynamics of *mh02* and *mh20* are not plotted completely for the year 2015, because there is a large jump in displacement due to a small debris fall event with a volume of a few cubic meters of rock in early summer (18 May 2015). For location *mh02*, the crackmeter installation continued measuring reliably, while the thermistor got damaged by the falling rocks with a resulting interruption in the temperature time series. After this debris fall event, the fracture at location *mh02* continued to deform with several small steps until late summer (14 August 2015) when the rock instrumented broke off completely during a bad weather period (see Fig. 10). The variable patterns of fracture deformation observed (Fig. 5) indicate that a field site can not be described by a single measurement location and a short measurement

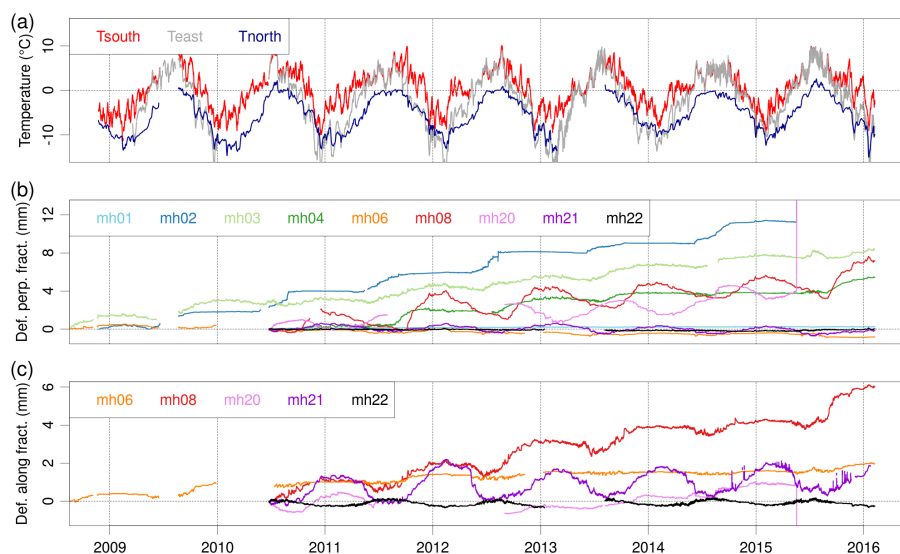


Figure 5. Time series of the thermal conditions and fracture deformation at the field site Matterhorn Hörnligrat with up to seven years of data. The thermal conditions are represented by rock temperatures for south, east and north side at 0.85 m depth. The relative fracture dynamics is represented perpendicular to and along fracture. A gap in the rock temperature time series of location *mh12* (T_{east}) is filled for the time period November 2012 until July 2013 and from August 2014 onwards applying the temperature gap filling method with a correlation coefficient $R^2 = 0.92$.

period. Therefore, monitoring of several fractures is essential to observe different modes of motion and accordingly to improve the process understanding of the fracture dynamics.

In the following paragraph, we analyze selected locations in more detail, namely *mh02* (South), *mh03* (North) and *mh08* (East, on ridge). These were chosen for their contrasting modes of deformation and their variations in aspect and cover all 5 different patterns of observed fracture dynamics.

5.1 Thermo-elastic response and LRM

Figure 6 shows the relationship and evolution between fracture dynamics and rock temperature. Applying the LRM, we obtain the linear regression coefficients that describe the reversible temperature dependent fracture deformation indicated with a black line in Figure 6. The fracture deformation at location *mh02* (South, Fig. 3) is almost temperature independent (regression coefficient of $5 \cdot 10^{-2} \text{ mm}/100^\circ \text{ C}$) except for the winters 2008/2009 and 2014/2015. In contrast, location *mh03* (North, Fig. 3) shows a stronger temperature dependency of $-3.0 \text{ mm}/100^\circ \text{ C}$. At *mh08* (East, Fig. 3), the coefficients are with $-9.0 \text{ mm}/100^\circ \text{ C}$ perpendicular to fracture and $-1.8 \text{ mm}/100^\circ \text{ C}$ along fracture even higher. These temperature dependencies are likely influenced by the combination of geometric arrangement and acting forces. The lack of temperature dependency in the LRM analysis, e.g. at location *mh02*, means that no reversible deformation caused by thermo-mechanical induced strain occurs. Or in other words, 15 irreversible deformation dominates.

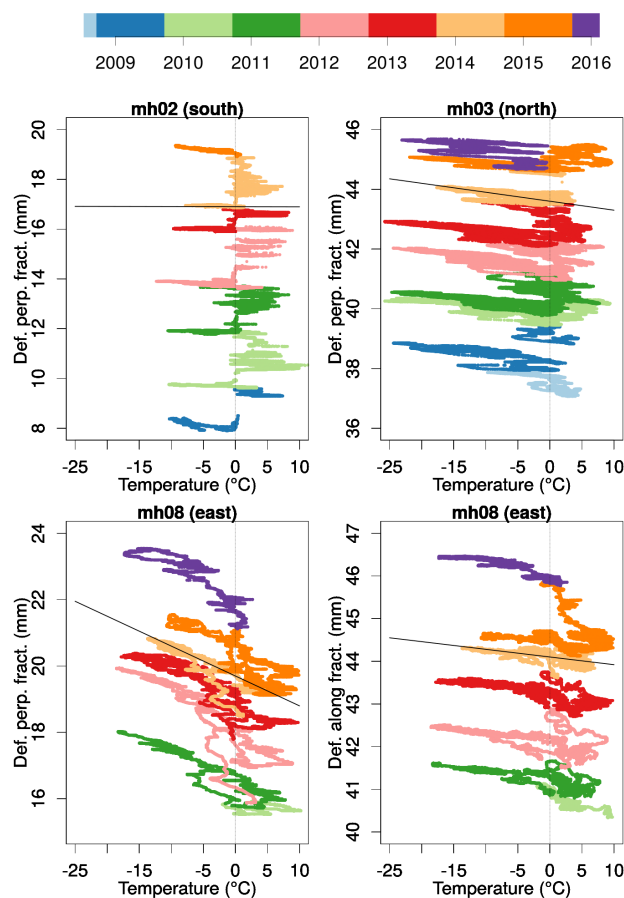


Figure 6. Temperature dependency of fracture deformation for location *mh02* (perp. fract.), *mh03* (perp. fract.) and *mh08* (perp. and parallel fract.). Discrete colors indicate hydrological years (1 October – 30 September). Black lines indicate the linear regression coefficient defined by the LRM.

5.2 Piecewise linear trend and LRM+

We model the reversible movement with the *LRM* (see green lines in Fig. 7) using the training phase in winter 2013/2014 (light blue shading in Fig. 7). The total fracture dynamics approximated with the *LRM+* model is shown in red and results from the *LRM* added to the piecewise linear trend. Note that for producing the *LRM+* deformation data (red line), only the temperature data, a few months of training data and 1 winter value of fracture deformation. With this reduced data input, the original fracture deformation is well reproduced including short term variations.

This analysis clearly show that we are able to describe the evolution of irreversible deformation by phases of quiescence followed by phases of linear irreversible deformation. For most locations, including *mh03*, this irreversible phase occurs during



summer, starting when rock temperatures reach above zero. This likely indicates thawing related processes, such as melt water percolation into fractures, cause this irreversible deformation. At a few locations, such as *mh08*, this linear irreversible phase occurs in autumn when rock temperatures drop below zero. Assuming water is available, this points to cryogenic processes (i.e. ice pressure, see Section 2) as likely cause irreversible fracture deformation.

- 5 There are however some discrepancies between the LRM+ and the measured signal. For example for location *mh03* (see Fig. 7a, black arrows) additional small excursions occur in summer 2010 and 2015, when summer temperatures are exceptionally high. Although these excursions seem reversible, they are not explained by thermo-mechanical induced strain (LRM). For location *mh08* in summer, the full amplitude of reversible deformation is not always reproduced.

5.3 Thawing degree days and summer offset

- 10 The summer offset of the fracture dynamics (OFST) and the thawing degree days (TDD) are parameters, which allow to analyze and interpret the inter-annual evolution (Fig. 8). TDD are not computed if the temperature time series contain a gap during summer. For most, a rough correspondence between OFST and TDD seems visible and some distinctive discrepancies are observed. For locations with aspect to the north and east, a correlation is apparent (negative for location *mh03*). Hinting on a substantial influence of rock temperature and therefore incoming conductive energy fluxes. Interestingly, at location exposed
15 to the south, OFST seems independent of TDD.

Summers with very high TDD, such as in 2015, although showing the highest OFST values, result in a local break-off at one location (*mh02*, see Section 5). The opposite behavior is observed for summer 2014, when TDD were exceptionally low due to a cold summer, and the summer offset low as well.

5.4 Irreversibility index

- 20 The irreversibility index (see Fig. 9) indicates the onset of irreversible deformation perpendicular to fracture. High index values can be observed in summer (temperature above zero) at location *mh02* (South) and *mh03* (North), during thawing period, while in winter low indices occur without any peaks (see Fig. 9a and 9b). The irreversibility index indicates that irreversible motion is influenced by warm temperatures, which further supports our findings from the relationship between OFST and TDD (Fig. 8).

- 25 In contrast, for location *mh08* high irreversible index occurs in autumn when temperatures are dropping below zero degrees, suggesting freezing processes. Note, these periods of high indices match the creeping phase obtained from the LRM+.

The earlier mentioned reversible excursions from the LRM+ at location *mh03* in summer 2010 and 2015 are picked up by increased indices. However, they are reversible deformations that are not represented by the LRM. This points to a potential additional reversible process that can not be explained by the thermo-mechanical induced strain.

6 Discussion

- 30 This study aims to investigate the relationship between thermo-mechanical forcing and deformation and to separate irreversible from reversible processes. The presented conceptual model describes the dominating processes leading to fracture dynamics in

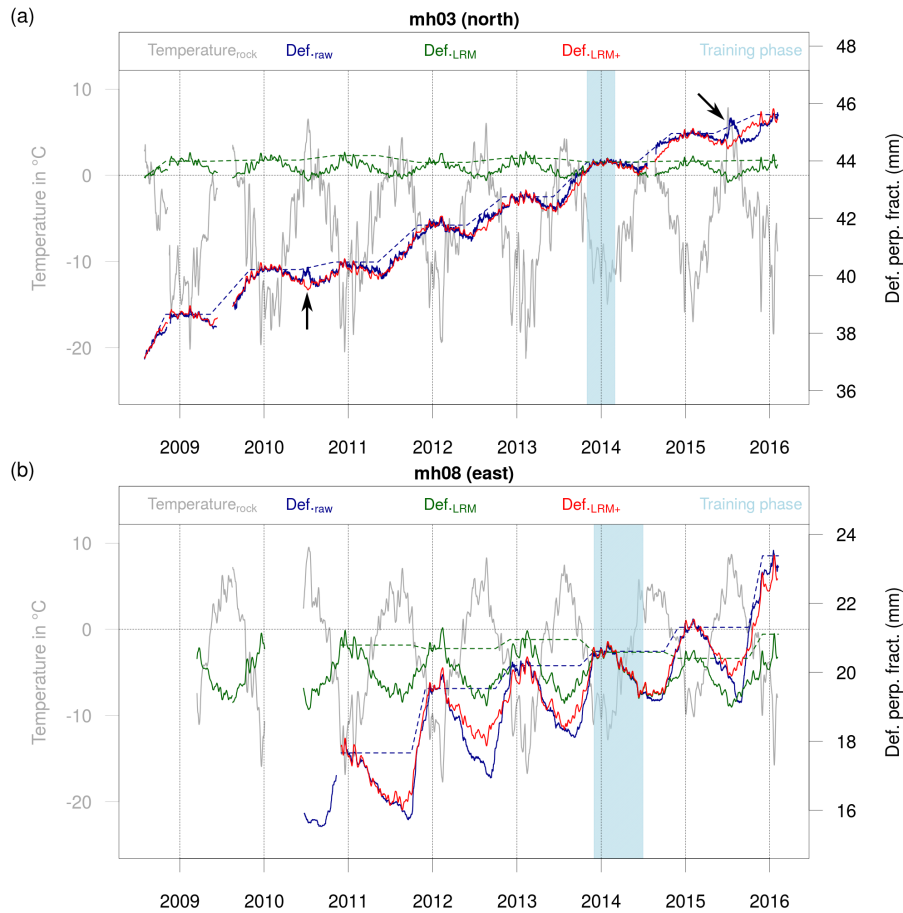


Figure 7. LRM (green) and LRM+ (red) applied to the deformation perpendicular to the fracture at location *mh03* (a) and *mh08* (b). Raw deformation measurements perpendicular to fracture (blue). The reversible component (green) due to thermo-elastic induced strains in rock can be modeled by a linear regression model (LRM) with temperature as input data (dark gray) and deformation measurements during a training period of several months (light blue shading). The combination of the LRM (green) and the piecewise linear deformation trend (blue dotted line, given by a reversible and creep phase, a fracture deformation measurement in each reversible phase and a linear interpolation in the creep phase) results in the modeled fracture deformation LRM+ (red).

steep bedrock permafrost and builds the basis for isolating different processes from the field observations. Possible interactions between the different processes are not considered. With the quantitative approach we developed here, we are able to separate reversible from irreversible fracture dynamics and produced a new irreversibility index, which is a novel metric for assessing rock wall stability.

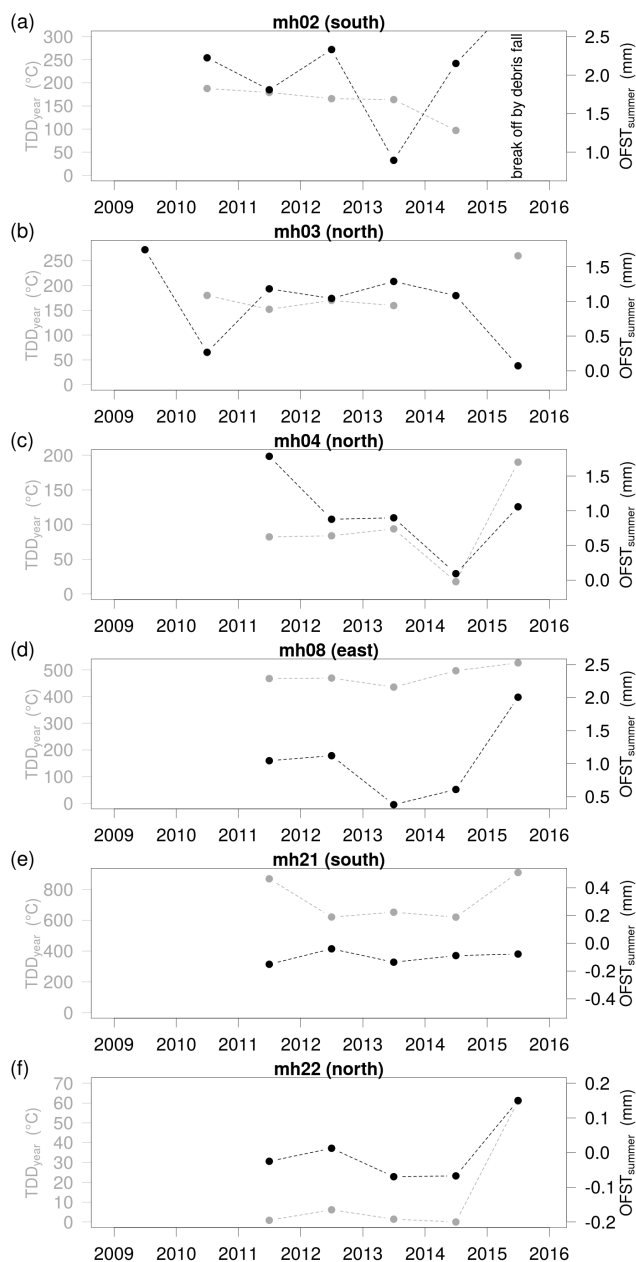


Figure 8. Inter-annual variability of thawing degree days (TDD) and summer offset of fracture deformation (OFST) perpendicular to fracture for all locations, except for location *mh20* due to many data gaps. Data at location *mh02* is missing from 2015 onwards due to the break-off and the TDD value at location *mh02* for the year 2014 is removed due to missing measurements.

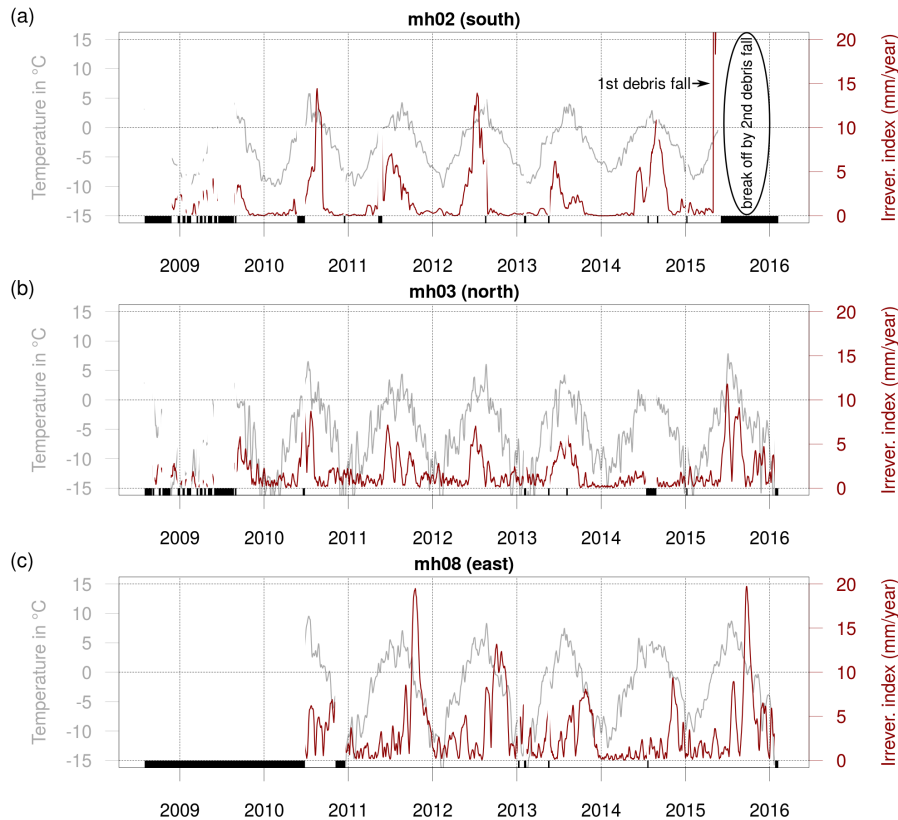


Figure 9. Irreversibility index for (a) location *mh02* (south), (b) location *mh03* (North) and (c) location *mh08* (East, on ridge) as an indicator for periods, where the irreversible movement is dominating. Black bars indicate periods where no or reduced data is available.

6.1 Separation of the reversible fracture deformation

Based on thermo-mechanical induced strain, using the LRM we are able to describe the observed reversible deformation component at all fractures instrumented. This confirms the assumption of periods with negligible irreversible movement. Further our analysis shows that one single such quiescent phase (training phase) is representative for the reversible component in deformation for the whole time series. The exception is at location *mh02* (see Fig. 10) where almost no reversible motion occurs
 5 apart from winter 2014/2015 after which the small failure event occurred.

The process of ice formation can also cause fracture opening with decreasing temperature, but the closing phase would have to start at the onset melting, which is clearly not observed. This leads to the conclusion that ice formation is not playing a dominant role for reversible fracture deformation.

10 The amplitude of reversible deformation varies strongly from location to location. Although we expect the thermal expansion coefficient of the rock material to be very similar, we explain this variation by highly variable volume or length of rock wall material influencing an individual fracture and the spatial heterogeneity in thermal conditions at depth vary spatially.



Reversible motion, which is not caused by thermo-mechanical forcing, is observed in summer 2010 as well as in summer 2015 at location *mh03*. This reversible motion is also visible in the irreversibility index in Fig. 9 with high values and may be caused by a non-local effect or points to an unidentified process causing reversible motion.

6.2 Inter-annual pattern of irreversible fracture deformation

5 Almost a decade of field measurement provides enough data for inter-annual analysis of fracture deformation. In general, all instrumented locations show a trend of fracture opening, but at variable rate between locations. At each individual location, the temporal pattern of deformation is very similar every year, but the irreversible summer offset (OFST) slightly varies over time. According to our analysis, this summer offset seems to correlate slightly with an increasing total amount of energy available (TDD). This implies that further warming and therefore increasing TDD's cause thawing of permafrost at greater
10 depth, potentially leading to an increase of summer offsets (OFST).

Percolating water allows effective heat transport along fractures leading to faster temperature increase in fractured rock mass than in intact rock. Additionally, percolation can affect the shear resistance along fractures and lead to a decrease of cohesion and friction, which may cause irreversible deformation. For example at location *mh02*, enhanced availability of water from snow melt after summer snowfall events seems to cause accelerated irreversible deformation, whereby this observation can not
15 be described with the piecewise irreversible motion of the LRM+ (see Fig. 10).

As TDD is defined using mean daily rock temperature, relationship between summer offset and TDD in south exposed rock should be interpreted carefully: Rapid variation of temperature with short peaks above 0° C can lead to thawing activity whereas the mean daily temperature stays below 0° C. This is often the case at locations exposed to strong solar radiation (south facing), even at winter time, and might explain why the TDD at the south exposed locations do not correlate with the summer
20 offset (e.g. *mh02* or *mh21*).

The presented summer offset only provides total deformation between two winters without any intra-annual information. In contrast, the irreversibility index is a proxy of impending rockfall activity and reveals information on the short term evolution of the irreversible fracture deformation all year round, even if the total summer offset (OFST) deformation is small. Even if such an index is based on local measurement, it can help to identify periods of enhanced creep or risk for failure. For example,
25 a strong increase was observed in early summer 2015 at location *mh02*, followed by several small rockfalls (approx. 2 – 3 m³) and a final break-off (Fig. 9a). Similar at location *mh03*, irreversible creep occurs during the melting period, which likely links a reduction of friction and cohesion along a fracture line.

However, there are also irreversibility index peaks in autumn, e.g. at location *mh08* (East, on ridge, Fig. 9c), which do not correlate with thawing days but with rapidly cooling and freezing in autumn. In this case, the growth of ice in late autumn acts
30 as a driving factor (Fig. 1 D3) through increasing ice pressure by volumetric expansion. In this case, if the ice melts in the subsequent summer, the fracture does not observed to close due to missing compressing force.

This study confirms the hypothesis of Hasler et al. (2012) that at the time was based on a much more limited data set.



6.3 Environmental controlling of irreversible fracture deformation

Our analysis of LRM+ and the irreversibility index both support the idea that there are distinct periods of solely reversible deformation periods with additional irreversible deformation. Irreversible deformation seems to be strongly linked to environmental conditions of, either rock temperature above zero degrees (indicating thawing) or less common periods of freezing conditions, whereby the piecewise linear trend introduced also fits this modal behavior. In the main winter time (temperatures well below zero) after the initial cooling phase, none of the fractures instrumented show irreversible motion. Water pressure is likely a marginal process at the Matterhorn field site, because the water can easily drain through the strongly fractured rock and the water availability is limited.

7 Conclusions

10 Knowledge of processes and factors affecting slope stability is essential for detecting and monitoring potentially hazardous slopes. Here we present a unique 7 year time series of fracture deformation, providing new insights on fracture dynamics in relation to thermal conditions on steep high-alpine rock slopes. The intra- and inter-annual behavior of the fracture dynamics strongly varies between locations, but patterns at individual locations are consistent over the entire observation period of several years. This implies that longterm monitoring at multiple fractures is essential to improve the process understanding of fracture dynamics.

15 The proposed LRM approach provides a tool for systematic analysis of fracture deformation and was successful in separating reversible from irreversible motion. After the removal of the reversible deformation component by LRM, we constructed the irreversibility index as a new metric that allows the detection of irreversible motion and link it to environmental forcing. Seven years of relative surface displacement measurements show that reversible fracture deformation caused by thermo-elastic induced strains of the material is occurring at all location all year round apart from one. In addition phases irreversible deformation with a stepwise behavior occur mostly during periods with temperature above zero degrees suggesting a decrease of cohesion and friction along fractures as a responsible process. At one location, ice formation due to freezing during the onset of the winter also causes irreversible deformation. These results are confirmed by the developed irreversibility index.

20 However, this approach to measure relative surface displacement has limited time resolution and provides only information from surface with a bad spatial coverage, which could get considerably improved by micro-seismic measurements.



Appendix A: Supplementary figure

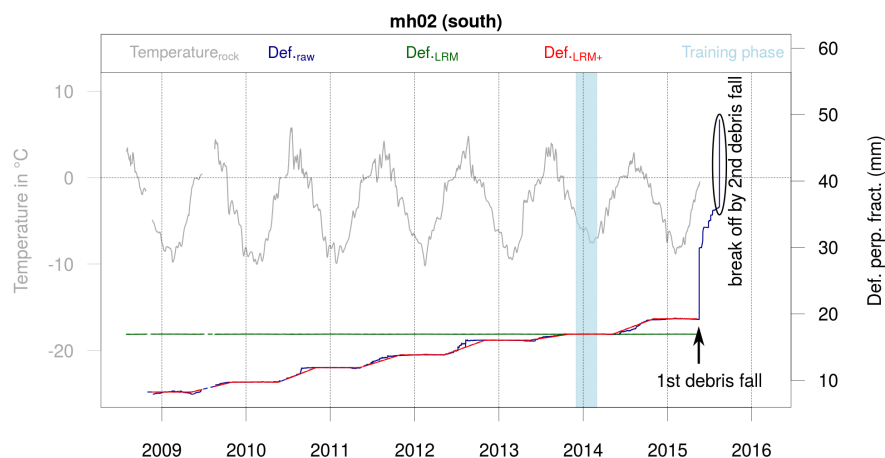


Figure 10. LRM (green) and LRM+ (red) applied to the deformation perpendicular to the fracture at location *mh03* (a) and *mh08* (b). Raw deformation measurements perpendicular to fracture (blue). The reversible component (green) due to thermo-elastic induced strains in rock can be modeled by a linear regression model (LRM) with temperature as input data (dark gray) and deformation measurements during a training period of several months (light blue shading). The combination of the LRM (green) and the piecewise linear deformation trend (blue dotted line, given by a reversible and creep phase, a fracture deformation measurement in each reversible phase and a linear interpolation in the creep phase) results in the modeled fracture deformation LRM+ (red). The discrepancies between the LRM+ and the field measurements occur during melting periods can not be described with the piecewise irreversible motion of the LRM+.

Appendix B: Data availability

All used data (processed and aggregated as 10 min averages) is available in the supplementary as csv-file for each location. Additional data can be accessed via the PermaSense GSN data portal (data.permasense.ch). A system documentation and tutorial for online data access is available on the PermaSense project web page (www.permasense.ch/data-access/permasense-data.html).

Author contributions. Jan Beutel and Andreas Hasler designed the field experiment and installed the sensors in 2010 and 2012. Jan Beutel and Samuel Weber have done maintenance work and data management tasks since spring 2012. The analysis code in R was written by Andreas Hasler and Samuel Weber. Samuel Weber developed the model code as well as the irreversibility index and performed the figures. Samuel Weber prepared the manuscript with substantial contribution of all co-authors.

Acknowledgements. We thank Max Maisch for providing us geomorphic considerations for Fig. 2. We acknowledge the PermaSense team, namely Tonio Gsell and Christoph Walser, who provided valuable support with the development of measurement devices, in the field and



with data management. The work presented in this paper was scientifically evaluated by the SNSF, and financed by the Swiss Confederation and by nano-tera.ch.



References

- Arosio, D., Longoni, L., Papini, M., Scaioni, M., Zanzi, L., and Alba, M.: Towards rockfall forecasting through observing deformations and listening to microseismic emissions, *Natural Hazards and Earth System Science*, 9, 1119–1131, doi:10.5194/nhess-9-1119-2009, 2009.
- Beutel, J., Gruber, S., Hasler, A., Lim, R., Meier, A., Plessl, C., Talzi, I., Thiele, L., Tschudin, C., Woehrl, M., and Yucel, M.: PermaDAQ: a scientific instrument for precision sensing and data recovery in environmental extremes, in: *The 8th ACM/IEEE International Conference on Information Processing in Sensor Networks*, San Francisco, California, USA, 2009.
- 5 Blikra, L. H. and Christiansen, H. H.: A field-based model of permafrost-controlled rockslide deformation in northern Norway, *Geomorphology*, 208, 34–39, doi:10.1016/j.geomorph.2013.11.014, 2014.
- Davidson, G. and Nye, J.: A photoelastic study of ice pressure in rock cracks, *Cold Regions Science and Technology*, 11, 141–153, doi:10.1016/0165-232X(85)90013-8, 1985.
- 10 Davies, M., Hamza, O., and Harris, C.: The effect of rise in mean annual temperature on the stability of rock slopes containing ice-filled discontinuities, *Permafrost and Periglacial Processes*, 12, 137–144, doi:10.1002/ppp.378, 2001.
- FOEN, Federal Office for the Environment: Map of potential permafrost distribution in Switzerland, www.bafu.admin.ch/naturgefahren/06140/06149/, 2005.
- 15 Gischig, V., Moore, J. R., Evans, K., Amann, F., and Loew, S.: Thermomechanical forcing of deep rock slope deformation: 1. Conceptual study of a simplified slope, *Journal of Geophysical Research*, 116, F04 010, doi:10.1029/2011JF002006, 2011.
- Gruber, S. and Haerberli, W.: Permafrost in steep bedrock slopes and its temperature-related destabilization following climate change, *Journal of Geophysical Research*, 112, F02S18, doi:10.1029/2006JF000547, 2007.
- Gruber, S., Hoelzle, M., and Haerberli, W.: Permafrost thaw and destabilization of Alpine rock walls in the hot summer of 2003, *Geophysical Research Letters*, 31, L13 504, doi:10.1029/2004GL020051, 2004.
- 20 Haerberli, W.: On the morphodynamics of ice/ debris-transport systems in cold mountain areas, *Norsk Geografisk Tidsskrift*, 50, 3–9, doi:10.1080/00291959608552346, 1996.
- Hall, K., Thorn, C. E., Matsuoka, N., and Prick, A.: Weathering in cold regions: some thoughts and perspectives, *Progress in Physical Geography*, 26, 577–603, doi:10.1191/0309133302pp353ra, 2002.
- 25 Hallet, B., Walder, J., and Stubbs, C.: Weathering by segregation ice growth in microcracks at sustained subzero temperatures: Verification from an experimental study using acoustic emissions, *Permafrost and Periglacial Processes*, 2, 283–300, doi:10.1002/ppp.3430020404, 1991.
- Hasler, A., Gruber, S., Font, M., and Dubois, A.: Advective heat transport in frozen rock clefts: Conceptual model, laboratory experiments and numerical simulation, *Permafrost and Periglacial Processes*, 22, 378–389, doi:10.1002/ppp.737, 2011.
- 30 Hasler, A., Gruber, S., and Beutel, J.: Kinematics of steep bedrock permafrost, *Journal of Geophysical Research*, 117, F01 016, doi:10.1029/2011JF001981, 2012.
- Huybrechts, P. and Oerlemans, J.: Reponse of the Antarctic Ice Sheet to future greenhouse warming, *Climate Dynamics*, 5, 93–102, doi:10.1007/BF00207424, 1990.
- Jia, H., Xiang, W., and Krautblatter, M.: Quantifying rock fatigue and decreasing compressive and tensile strength after repeated freeze-thaw cycles, *Permafrost and Periglacial Processes*, doi:10.1002/ppp.1857, 2015.
- 35 Jomelli, V., Brunstein, D., Grancher, D., and Pech, P.: Is the response of hill slope debris flows to recent climate change univocal? A case study in the Massif des Ecrins (French Alps), *Climatic Change*, 85, 119–137, doi:10.1007/s10584-006-9209-0, 2007.



- Keuschnig, M., Hartmeyer, I., Höfer-Öllinger, G., Schober, A., Krautblatter, M., and Schrot, L.: Permafrost-related mass movements: Implications from a rock slide at the Kitzsteinhorn, Austria, in: *Engineering Geology for Society and Territory*, edited by Lollino, G., Manconi, A., Clague, J., Shan, W., and Chiarle, M., vol. 1, chap. 48, pp. 255–259, Springer International Publishing Switzerland, doi:10.1007/978-3-319-09300-0_48, 2015.
- 5 Krautblatter, M., Huggel, C., Deline, P., and Hasler, A.: Research Perspectives on Unstable High-alpine Bedrock Permafrost: Measurement, Modelling and Process Understanding, *Permafrost and Periglacial Processes*, 23, 80–88, doi:10.1002/ppp.740, 2012.
- Krautblatter, M., Funk, D., and Günzel, F.: Why permafrost rocks become unstable: a rock-ice-mechanical model in time and space, *Earth Surf. Process. Landforms*, 38, 876–887, doi:10.1002/esp.3374, 2013.
- Matsuoka, N.: Mechanisms of rock breakdown by frost action – an experimental approach, *Cold Regions Science and Technology*, 17, 253–270, 1990.
- 10 Matsuoka, N.: Direct observation of frost wedging in alpine bedrock, *Earth Surface Processes and Landforms*, 26, 601–614, doi:10.1002/esp.208, 2001.
- Matsuoka, N. and Murton, J.: Frost weathering: recent advances and future directions, *Permafrost and Periglacial Processes*, 19, 195–210, doi:10.1002/ppp.620, 2008.
- 15 Mellor, M.: Mechanical properties of rocks at low temperatures, in: *2nd International Conference on Permafrost*, Yakutsk, pp. 334–344, International Permafrost Association, 1973.
- Murton, J., Peterson, R., and Ozouf, J.-C.: Bedrock fracture by ice segregation in cold regions, *Science*, 314, 1127–1129, doi:10.1126/science.1132127, 2006.
- Nordvik, T., Blikra, L. H., Nyrnes, E., and Derron, M.-H.: Statistical analysis of seasonal displacements at the Nordnes rockslide, northern Norway, *Engineering Geology*, 114, 228–237, doi:10.1016/j.enggeo.2010.04.019, 2010.
- 20 Pogrebiskiy, M. and Chernyshev, S.: Determination of the permeability of the frozen fissured rock massif in the vicinity of the Kolyma hydroelectric power station, *Cold Regions Research and Engineering Laboratory – Draft translation*, 634, 1–13, 1977.
- Schär, C., Vidale, P., Lüthi, D., Frei, C., Häberli, C., Liniger, M., and Appenzeller, C.: The role of increasing temperature variability in European summer heatwaves, *Nature*, 427, 332–336, doi:10.1038/nature02300, 2004.
- 25 Sidle, R. C. and Ochiai, H.: Landslides: processes, prediction, and land use, vol. 18 of *Water Resources Monograph Series*, American Geophysical Union, Washington, DC, doi:10.1029/WM018, 2006.
- Staub, B., Hasler, A., Noetzi, J., and Delaloye, R.: Gap filling algorithm for ground surface temperature data, *Permafrost and Periglacial Processes*, in review, 2015.
- Terzaghi, K.: Stability of steep slopes on hard unweathered rock, *Géotechnique*, 12, 251–270, doi:10.1680/geot.1962.12.4.251, 1962.
- 30 Walder, J. and Hallet, B.: A theoretical model of the fracture of rock during freezing, *Geological Society of America Bulletin*, 96, 336–346, doi:10.1130/0016-7606(1985)96<336:ATMOTF>2.0.CO;2, 1985.
- Watson, A. D., Moore, D. P., and Stewart, T. W.: Temperature influence on rock slope movements at Checkerboard Creek, in: *Proceedings of the ninth International Symposium on Landslides*, vol. 2, p. 1293–1298, 2004.
- Wegmann, M. and Gudmundsson, G. H.: Thermally induced temporal strain variations in rock walls observed at subzero temperatures, in: *Advances in old-region thermal engineering and sciences*, edited by Hutter, K., Wang, Y., and Beer, H., vol. 533, pp. 511–518, Springer Berlin Heidelberg, doi:10.1007/BFb0104208, 1999.